

Variance in Bidirectional Reflectance over Discontinuous Plant Canopies

Wenge Ni,* Curtis E. Woodcock,* and David L. B. Jupp†

An exploratory study of the variance of the bidirectional reflectance over discontinuous plant canopies indicates that the patterns in variance can be related to the properties of the plant canopies. The spatial variance of the bidirectional reflectance calculated from ASAS images shows peak values at the hotspot and near nadir. This behavior can be explained by the geometric effect of discontinuous tree crowns and the regularization effect. Validation of Jupp and Woodcock's two-component geometric optical (GO) model (1992) shows that it captures the basic features of the spatial variance of the bidirectional reflectance over discontinuous plant canopies. Their two-component GO model is modified to account for the spatial interactions of four scene components. Validation shows that the modified GO model improves predictions. This exploratory study will benefit future use of directional imagery to recover surface parameters by helping characterize the distributional properties of directional imagery. ©Elsevier Science Inc., 1999

INTRODUCTION

There has been much work in the last two decades on bidirectional reflectance distribution functions (BRDF), both in terms of measurement and modeling [see the review by Strahler (1997)]. One of the primary benefits of an improved understanding of the properties of BRDFs should be the ability to improve recovery of surface properties from directional imagery. Until recently only relatively small amounts of directional imagery have been available, primarily from aircraft borne sensors such as ASAS (Irons et al., 1991) and the airborne POLDER

(Deschamps et al., 1994) instruments. Also, directional measurements have been made in a variety of laboratory or field settings. However, soon there will be considerable directional imagery available, particularly from the MISR (Diner et al., 1989) and MODIS (Ardanuy et al., 1991) instruments. Thus, the opportunity for recovery of surface parameters from directional measurements will increase dramatically.

With the notion of recovery of surface parameters based on directional reflectance comes the idea that BRDFs are the first-order directional properties of a landscape. Often critical to inversion processes and their success are the second-order directional properties. Local spatial variance and large, anisotropic change in recorded radiance with changing Sun position and sensor view angle are characteristic of images of woodlands and forest areas. In these ecosystems, the canopy is discontinuous, or "gappy," and the local spatial and viewing angle variation in images is created by a number of ecologically significant factors. These include interactions between the discrete nature of the canopy, the high natural spatial variation in canopy, the high natural spatial variation in canopy structure, and the visible shadowing effects as the Sun and view positions vary.

The BRDF of forests and woodlands is a statistical function which operates at the scale of an average patch of cover rather than at the scale of crowns. Studies of the forests and woodlands using aerial photography and high spatial resolution scanner data show very high variance at this detailed scale. In addition, the directional effects of the Sun and observer positions interact significantly to create an angular anisotropic variation. At the fine scale, surface variations cause the local intensity variation, or image texture. This variation or texture depends on both illumination and viewing direction, which was defined as BTF (bidirectional texture function) in Dana et al. (1996). Here this has been called the BRVF or bidirectional reflectance variance function, corresponding to BRDF (bidirectional reflectance distribution func-

* Department of Geography and Center for Remote Sensing, Boston University, Boston

† CSIRO Earth Observation Centre, Canberra, ACT, Australia

Address correspondence to Wenge Ni, Raytheon STX Corp., 4400 Forbes Blvd., Lanham, MD 2076. E-mail: ni@homer.stx.com

Received 22 May 1998; revised 23 November 1998.

tion). Statistically the *BRDF* (i, v, φ) and *BRVF* (i, v, φ) over a multiangular scene images are calculated as the mean and variance of the multiangular images in Eqs. (1) and (2):

$$BRDF(i, v, \varphi) = E(r(i, v, \varphi; k)) = \frac{1}{N} \sum_{k=1}^N r(i, v, \varphi; k), \quad (1)$$

$$BRVF(i, v, \varphi) = Var(r(i, v, \varphi; k)) \\ = \frac{1}{N-1} \sum_{k=1}^N (r(i, v, \varphi; k) - R(i, v, \varphi))^2, \quad (2)$$

where i, v and φ are the solar and viewing zenith angles and their relative azimuth angle, N is the pixel number of the multiangular scene images, and the lower case $r(i, v, \varphi, k)$ is the reflectance at pixel level. Spatial texture/variance is basically about patch and gap size distributions. How this changes with Sun and view angles is a significant “stereological” analysis of the 3D canopy structure. However, we really need to understand it more to use it.

Recently more and more studies on the spatial variation of images have drawn the attention of remote sensing science community. From theory and the real image analysis of the variograms of images, which describes the spatial variation of images as function of distance have shown the close relationship between variograms of images and the surface parameters. Studies by Woodcock et al. (1988a,b) and Jupp et al. (1988; 1989) using variograms and local variance showed that the spatial variances of images are closely related to the size and density of scene objects. The tools developed in their study can be used and extended for multiangular images.

Variogram analysis over digitized aerial video images by Cohen et al. (1990) showed that the range of semi-variograms based on 1-m spatial resolution related to the mean tree canopy sizes of the stands, the sills responded to the presence of vertical layering in the canopies and to percent canopy cover. Semivariograms based on 10 m and 30 m pixels contained significantly less useful information.

Wulder et al. (1998) retrieved LAI and NDVI and texture information-variogram empirically. The rationale behind is the texture information-vertical structure related to tree height distribution and horizontal distribution pertaining to stand density and spatial distribution of the trees.

Bruniquel-Pinel and Gastellu-Etchegorry (1998) used the discrete anisotropic radiative transfer (DART) model (Gastellu-Etchegorry et al., 1996) to simulate images in which the texture-variogram was quantified. Their study showed the complex dependence of variogram characteristics (range, sill, amplitude of oscillations) on biophysical and acquisition parameters. Due to the complicated DART model, the authors concluded it was difficult to extract reliable texture information from real remote sensing data.

One question concerns the importance of BRVFs. The importance of BRVFs will not become apparent until extensive evaluation of surface parameter retrievals based on directional measurements are conducted. The reason is that both the mean (BRDF) and variance (BRVF) of directional reflectance will influence the utility of directional measurements for recovering surface properties. In this regard, the experience in the spectral domain may prove relevant. Initial exploration of the first-order spectral properties of surface materials (or spectral signatures) frequently led to the expectation that these materials could be separated using multispectral imagery such as that collected by Landsat MSS or TM. For example, the means for different forest species or agricultural crops had distinctive spectral patterns. However, the inherent within class variances (or second-order spectral properties) often undermined mapping accuracies, and hence limited the utility of multispectral image classification. As the interest in using directional measurements to recover surface properties increases, the magnitude of the variance in directional reflectances will become increasingly important.

With respect to the inversion of canopy reflectance models for the extraction of the forest parameters, one problem that persists is that the density and size of trees are not separable from the directional mean radiance (BRDF) (Li and Strahler, 1996). This is unfortunate as there are many uses of tree size. For example, maps of tree size are needed for the management of a variety of resources by the U.S. Forest Service (Woodcock et al., 1994; 1997). Tree size also influences the radiation regime within forest canopies, which influences a number of surface physical processes (Ni et al., 1997). Using a descriptive model, the effect of variation of scene object sizes and densities on BRVFs were also analyzed (Ni, 1997). The simulation results indicate that the variation of the scene object size and density do affect the BRVFs differently. This indicates that useful tree size information may exist in BRVFs and thus separation of the effect of tree size and tree density based on BRVF values may be possible.

Recently attention has been devoted to second-order spatial statistics of images. The earliest study on this is Li and Strahler’s inversion model (Li and Strahler, 1985), in which the relationship between the spatial variances of images and forest structural parameters was investigated theoretically. Tree size can be inverted from the mean and variance of the crown area index $m = \lambda r^2$, where λ is the crown count density and r is the horizontal crown radius. This method has been used by Woodcock et al. (1994) for canopy structure mapping at the stand level. Total tree cover, or m , can be mapped effectively, but separation of count density and tree size based on inversion of the Li-Strahler model were poor. The primary reason is the inconsistent relationship between the spatial variance and tree size (Woodcock et al., 1994; 1997).

It should be noted that the work of Woodcock et al. (1994; 1997) was based on TM imagery with a single view angle, so that inversion based on BRDFs and multiangle data might improve tree size estimates. One of the interesting results of the present study is that there appear to be effects related to tree size in BRVFs, and hence incorporation of BRVFs might improve estimation of tree size.

The definition or use of second-order directional properties requires a higher level of organization in images above individual pixels. In essence, individual pixels must be viewed as samples from larger entities. For naturally vegetated landscapes these entities are usually patches or stands which are little more than polygons in images composed of a group of continuous pixels within which the properties of the vegetation are somewhat constant. Vegetation classes can also serve as a higher-level entity. For such multipixel objects the BRVF can be thought of as the pixel to pixel variability in the BRDF.

Little is known about the properties of BRVFs or the influence of variance on inversion processes based on directional properties of images. Jupp and Woodcock (1992) and Jupp (1997) studied the BRVF of a woodland in Australia using digitized aerial photographs and a simple two-component GO model of BRVFs. Beyond those efforts little is known about how variance changes as a function of viewing and illumination directions, or its causes. The purpose of this article is to explore BRVFs for boreal forest stands as an attempt to: 1) identify their basic characteristics, 2) determine if they can be related to the properties of vegetation canopies, and 3) evaluate the validity of Jupp's simple two-component model of the BRVF. One result is a modification of Jupp's model to incorporate the effect of more scene components. The first portion of this article is empirical and exploratory in nature and uses ASAS imagery over four forest stands. The second portion pursues models of BRVFs for one of these forest stands where the hotspot is best sampled in the ASAS imagery.

DIRECTIONAL IMAGERY

The boreal ecosystem-atmosphere study (BOREAS) has been undertaken to improve our understanding of the interactions between the boreal forest biome and the atmosphere, and to clarify the role of boreal forests in global climate change (Sellers et al., 1995). During the field campaigns of BOREAS, airborne multiangular images from the ASAS instrument were collected at selected locations, including an old black spruce stand (SOBS) (on 19 April 1994 and 21 July 1994), the old jack pine stand (SOJP) (on 21 July 1994) and the old aspen stand (SOA) (on 21 July 1994) in the southern super study area of BOREAS near Candle Lake, Saskatchewan. The solar zenith angle for the ASAS images on 21 July 1994 varies between 33.6° and 34.6°. There are six view-

ing zenith angles: -45°, -26°, 0°, 26°, 45°, 55° or 45°, 26°, 0°, -26°, -45°, -55°, depending on whether the airplane is heading toward the Sun or away from it. The positive values indicate the backward scattering direction and the negative values the forward scattering direction. There are no measurements close to the hotspot for the sets of images collected on 21 July 1994, but the images at viewing zenith angle 26° and 45° still show some hotspot effect (Fig. 1-4). The solar zenith angle for the ASAS images on 19 April 1994 is 47.7°. There are nine viewing zenith angles: -55°, -45°, -26°, -15°, 0°, 15°, 26°, 46°, 60°, and thus there is an image relatively close to the hotspot angle. The spatial resolution of the images varies as a function of viewing angle, with larger viewing angles having larger pixel sizes (Table 1).

The SOBS and SOJP sites are coniferous forests with mostly moss in the understory. The SOA site is broadleaf deciduous forest with a grass understory. Airphotos and field measurements show that the SOJP site is sparser than the SOBS site. The tree density is 0.16-0.24 m⁻² in the SOJP site and 0.37-0.44 m⁻² in the SOBS site. Tree heights range from 12 m to 15 m in the SOJP site versus 0-11 m in the SOBS site and the horizontal crown radius is 1.2 m in the SOJP site versus 0.76 m in the SOBS site (Chen, 1996). The trees are much bigger in the SOA site, as data collected during winter show that the tree average height is 21.5 m and the horizontal crown radius is 2.12 m. The crown count density is 0.114 m⁻² (Hardy et al., 1997).

To calculate the spatial variances of ASAS images, the portion of the images corresponding to the locations where the field measurements provided above was used. Since pixel size varies with view angle, the area associated with each stand was digitized for each view angle separately. The atmospheric correction code 6S (Vermote et al., 1997) was used to convert the DN values to reflectances. The mean (BRDF) and variance (BRVF) of the reflectance values for each stand area were calculated for each viewing angle.

Figures 1-4 show the calculated mean or BRDF, and variance or BRVF, for the different stands in red and near infrared from the ASAS measurements. There are both similarities among the BRDF plots and differences between the individual BRDF plots. The first similarity is that for all stands the BRDF exhibits a half-bowl shape (due to no angular sampling at larger viewing zenith angles, the other half bowl was not observed here) with a peak value at the hotspot case, that is, when the Sun and viewing directions are the same. This effect is due to the shadowing effect of tree crowns, leaves, and other canopy elements, where from forward scattering to backward scattering, there is a decrease in the observed shadows until no shadows can be seen when the Sun and the viewer direction coincide. Past the hotspot point, more shadows can be seen again and reflectance decreases. Second, the BRDF pattern in the red shows a

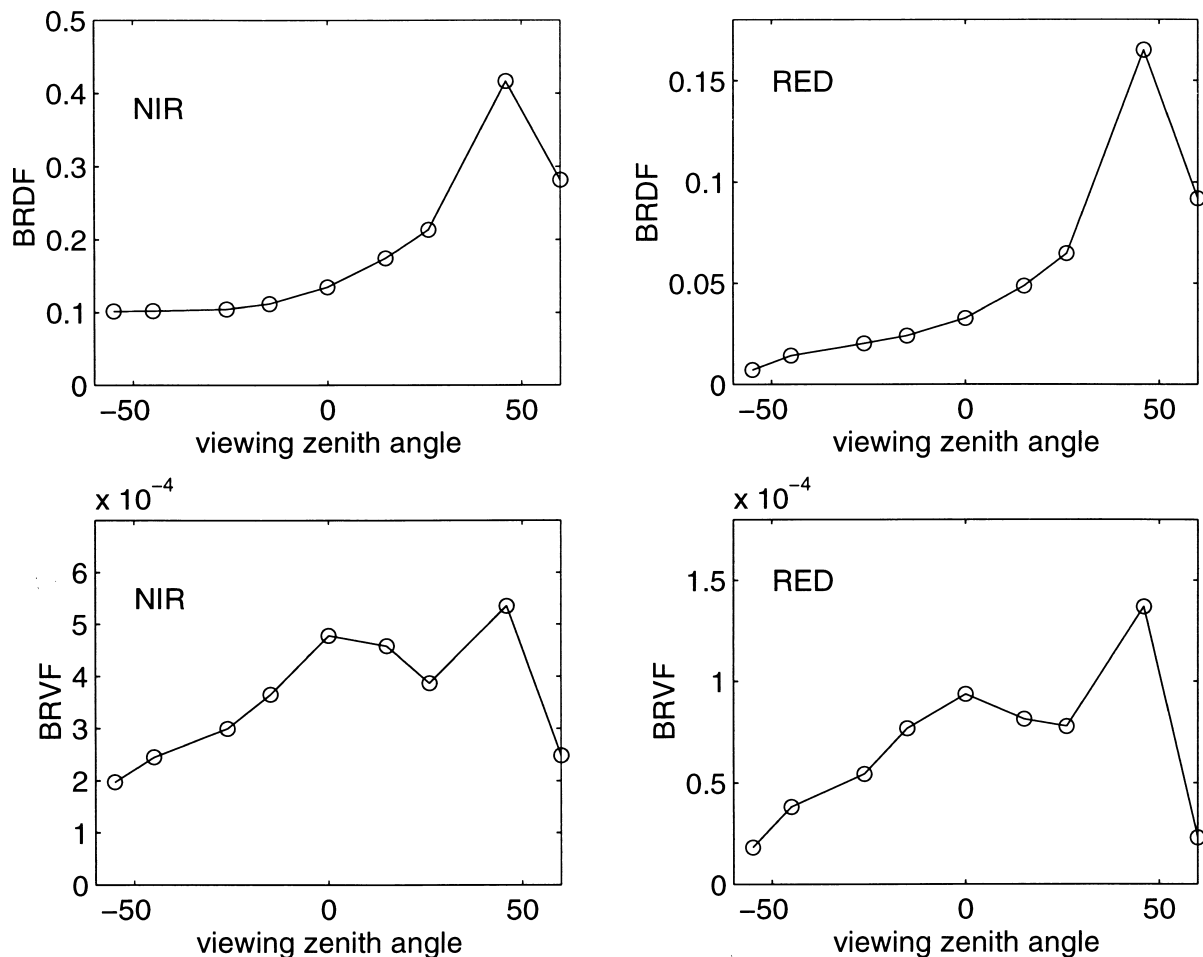


Figure 1. The BRDF and BRVF values calculated from ASAS images of the old black spruce (SOBS) forest stand in the southern study site of BOREAS on 19 April 1994.

somewhat stronger and sharper hotspot than in the near-infrared, and the overall reflectance values in near-infrared are higher than in the red. These effects are due to the higher absorption of green vegetation of red light. The higher single scattering albedo in the near-infrared leads to more multiple scattering, which results in brighter signatures for all scene components in the near-infrared than in the red. Since the hotspot effect occurs only for single scattering, the higher absorption at red wavelengths results in a stronger hotspot phenomenon in the red than in the near infrared.

There are also several differences. First, the ASAS image over the old black spruce stand collected on 19 April 94 shows a stronger hotspot than the other three plots. This is primarily due to better sampling of the hotspot on this date. Second, for the old aspen stand, there are much brighter BRDF values in the near-infrared than in red, and less of a crown hotspot is observed compared to other three stands. Since hotspots are mainly due to shadowing of canopy elements, including the crown level and leaf level, and the old aspen stand in a

more continuous canopy with a hazelnut understory, less shadowing of crowns is observed which leads to a weaker crown hotspot. The broad hotspot generated by discrete crowns and their shadows is weaker for this nearly continuous canopy. A narrow hotspot for leaves might exist, but is not sampled in the ASAS data.

The bottom two plots in Figures 1–4 show the BRVF as measured in the ASAS images for each stand. Several patterns are apparent, again including both similarities and differences. One similarity is that for all stands, the BRVF tends to have the peak values near nadir and/or the hotspot. Figure 1 shows a clear pattern of two peaks near nadir and the hotspot for both the red and the near infrared. The other three figures (3, 2, and 4) are less clear in this regard, which may be due to poor sampling of the hotspot in these ASAS images. For the red wavelengths, the maximum values occur near the hotspot, but also have high values at nadir. In the infrared, the maximum values occur at or near nadir, with values close to the hotspot direction also being generally larger than the opposite view angles. Only better sam-

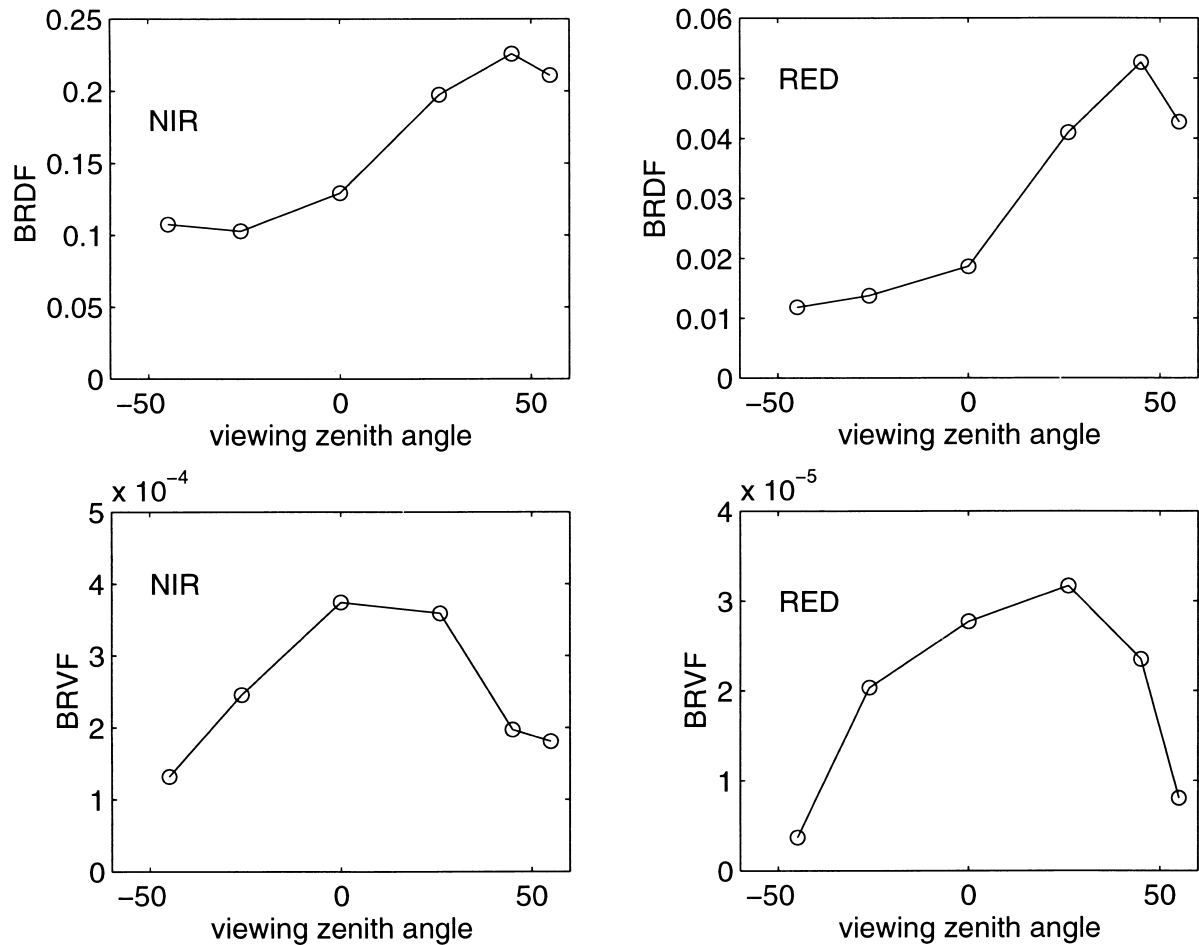


Figure 2. The BRDF and BRVF values calculated from ASAS images of the old black spruce (SOBS) forest stand in the southern study site of BOREAS on 21 July 1994.

pling of the hotspot would reveal whether or not the pattern of the two peaks observed in Figure 1 is common. The effect of two peaks in directional variance can be explained by the shadowing effect of tree crowns. Using the model for scenes from geometric optics, the scene in the field of view of the sensor is a mixture of four components, that is, sunlit crown, shaded crown, sunlit background, and shaded background. The interaction of these four components and the differences of their spectral signatures lead to the spatial variance of remote sensing images. The change of the areal proportions and their spectral signatures of these four components as a function of the Sun and viewing angles leads to the change of spatial variance with the Sun and viewing angles. Figures 5 and 6 show the areal proportions as estimated by geometric optics and their spectral signatures for the old black spruce stand as estimated using the methods developed in Ni et al. (1998). At nadir, Figure 5 shows more background, including a peak value for shaded background and a local peak value for sunlit background, and as a result the contrast is stronger. At the hotspot, Figure 5 shows that the contrast between

the two sunlit components is strong. Thus geometric effects can explain high BRVF values at the hotspot and near nadir.

The BRVF plot over the old jack pine stand shows larger BRVF values in the red than the old black spruce stand. This may be due to the fact that the background in old jack pine stand is brighter than the old black spruce stand (Ni et al., 1997; Miller et al., 1997). This leads to larger spectral contrasts between components and thus higher variance.

This is also another factor which influences the shape of these BRVFs, called the regularization effect. The reflected radiance within each pixel in an image is an integrated value over the area of a pixel, which is called regularization, or the averaging effect. The larger the pixel size is, the lower the variance will be (Woodcock et al., 1988a,b; Jupp et al., 1988; 1989). As shown above (Table 1), the spatial resolutions of the multiangular ASAS images become more coarse with an increase in the viewing zenith angles, and thus the BRVF values at higher viewing angles would be expected to be lower than those closer to nadir simply due to pixel size effects.

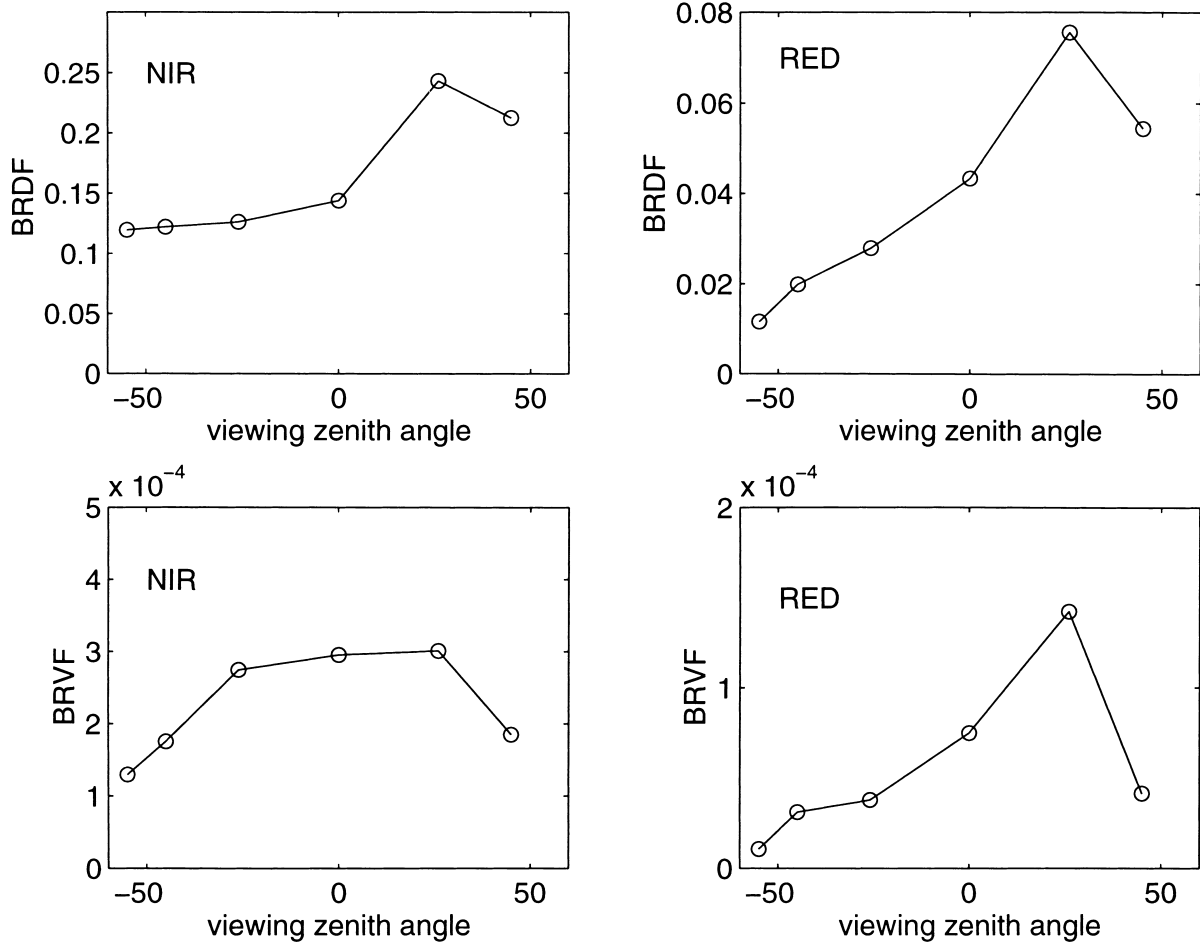


Figure 3. The BRDF and BRVF values calculated from ASAS images of the old jack pine (SOJP) forest stand in the southern study site of BOREAS on 21 July 1994.

MODELS

The only existing model that explicitly estimates BRVFs as a function of scene parameters was developed by Jupp and Woodcock (1992). One goal of this study is to determine the validity of this simple two-component model for boreal forests. The approach adopted is to compare ASAS directional measurements with model predictions for the SOBS site. For simplicity the effects of regularization have been ignored. While this comparison is not ideal, it does allow at least qualitative comparisons between the shapes of the observed and modeled BRVFs. Given that the pixel sizes of the ASAS images are relatively small compared to other remote sensing images such as Landsat TM images, the regularization effects should be small. Since regularization decreases variance, the effect would be an overall reduction of the model estimates of variance, with the reduction being somewhat larger at larger viewing angles.

The Simple Two-Component Model

In the GO model of Li and Strahler (1985), the forest canopy is treated as an assemblage of discrete tree crowns

of specific shape and size. The scene has four components: sunlit crowns, shaded crowns, sunlit background, and shaded background (see Fig. 7). The bidirectional reflectance of a single pixel, r , is modeled as the sum of radiances or reflectance of individual components as weighted by their areal proportions. In the simplified two-component model, the shaded background, sunlit tree, and shaded tree components are combined into one composite component so that Eq. (3) results:

$$\begin{aligned}
 r(i, v, \varphi) &= k_g(i, v, \varphi)G + k_c(i, v, \varphi)C \\
 &\quad + k_t(i, v, \varphi)T + k_z(i, v, \varphi)Z \\
 &= k_g(i, v, \varphi)G + (1 - k_g(i, v, \varphi))X \\
 &= X(i, v, \varphi) + k_g(i, v, \varphi)(G - X), \quad (3)
 \end{aligned}$$

where i, v, φ are incident and viewing zenith angles and their relative azimuth angle, $k_g(i, v, \varphi)$, $k_c(i, v, \varphi)$, $k_t(i, v, \varphi)$, and $k_z(i, v, \varphi)$ are the areal proportions of the sunlit background, sunlit crown, shaded crown, and shaded background, and G, C, T, Z are the spectral signatures of each component individually. The quantity X is a composite component combining sunlit and shaded tree and

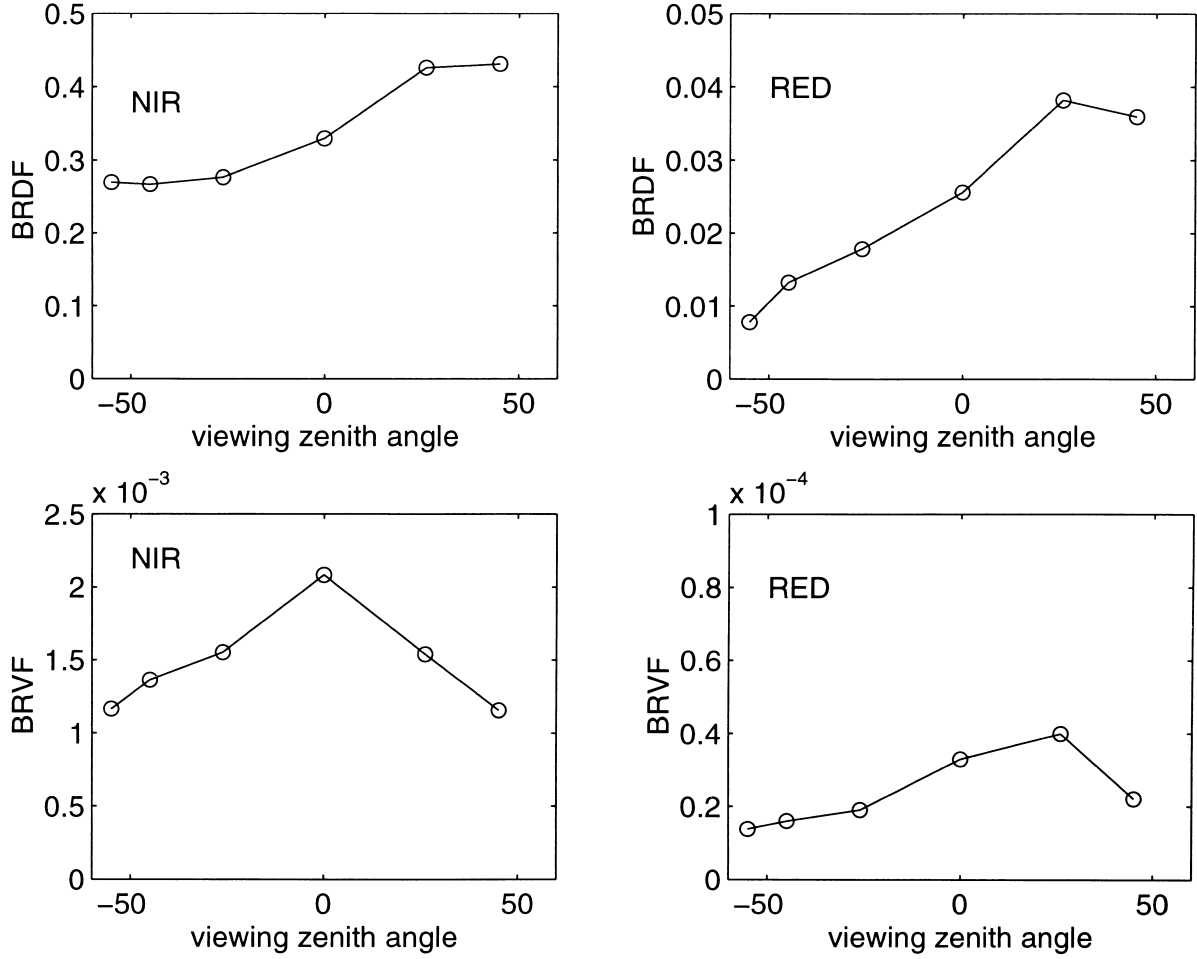


Figure 4. The BRDF and BRVF values calculated from ASAS images of the old aspen (SOA) forest stand in the southern study site of BOREAS on 21 July 1994.

shaded background as shown in Eq. (4):

$$X(i, v, \varphi) = \frac{k_c(i, v, \varphi)C + k_t(i, v, \varphi)T + k_z(i, v, \varphi)Z}{1 - k_g(i, v, \varphi)}. \quad (4)$$

This approach is intended for use in the red wavelengths where all three of these components are dark, and the contrast in the scene is primarily the result of the contrast between a bright sunlit background, $k_g(i, v, \varphi)$ and the dark trees and shadows.

Table 1. Spatial Resolution of ASAS Images

Viewing Zenith Angle (deg)	Spatial Resolution
-55	3.2 m by 5.4 m
-45	3.2 m by 4.4 m
-26	3.2 m by 3.4 m
-15	3.2 m by 3.2 m
0	3.2 m by 3.2 m
+15	3.2 m by 3.2 m
+26	3.2 m by 3.4 m
+45	3.2 m by 4.4 m
+60	3.2 m by 6.2 m

For such a model, the average radiance (e.g., BRDF) over all pixels in a patch with the same basic understory or background and tree structure is given in Eq. (5):

$$R(i, v, \varphi) = E(r(i, v, \varphi)) \\ = X(i, v, \varphi) + (G - X(i, v, \varphi))k_g(i, v, \varphi), \quad (5)$$

where $k_g(i, v, \varphi)$ is the mean value of $k_g(i, v, \varphi)$, or the expected proportion of sunlit background. Moreover, the variance of the pixel radiance for pixel size s is

$$\text{Var}_s(r(i, v, \varphi)) = (G - X(i, v, \varphi))^2 \text{Var}_s(k_g(i, v, \varphi)). \quad (6)$$

From this relationship it is clear that the variance of a scene is defined by that of $k_g(i, v, \varphi)$ and the contrast between the sunlit background and the composite of tree and shadow.

In the simplified model, the viewed scene consists of objects that are a composite of projected tree-plus-shadow silhouettes scattered over a sunlit background. The sensor integrates the radiance over a pixel so the model for the resulting image is one of objects on a contrasting background regularized by integration over pixels.

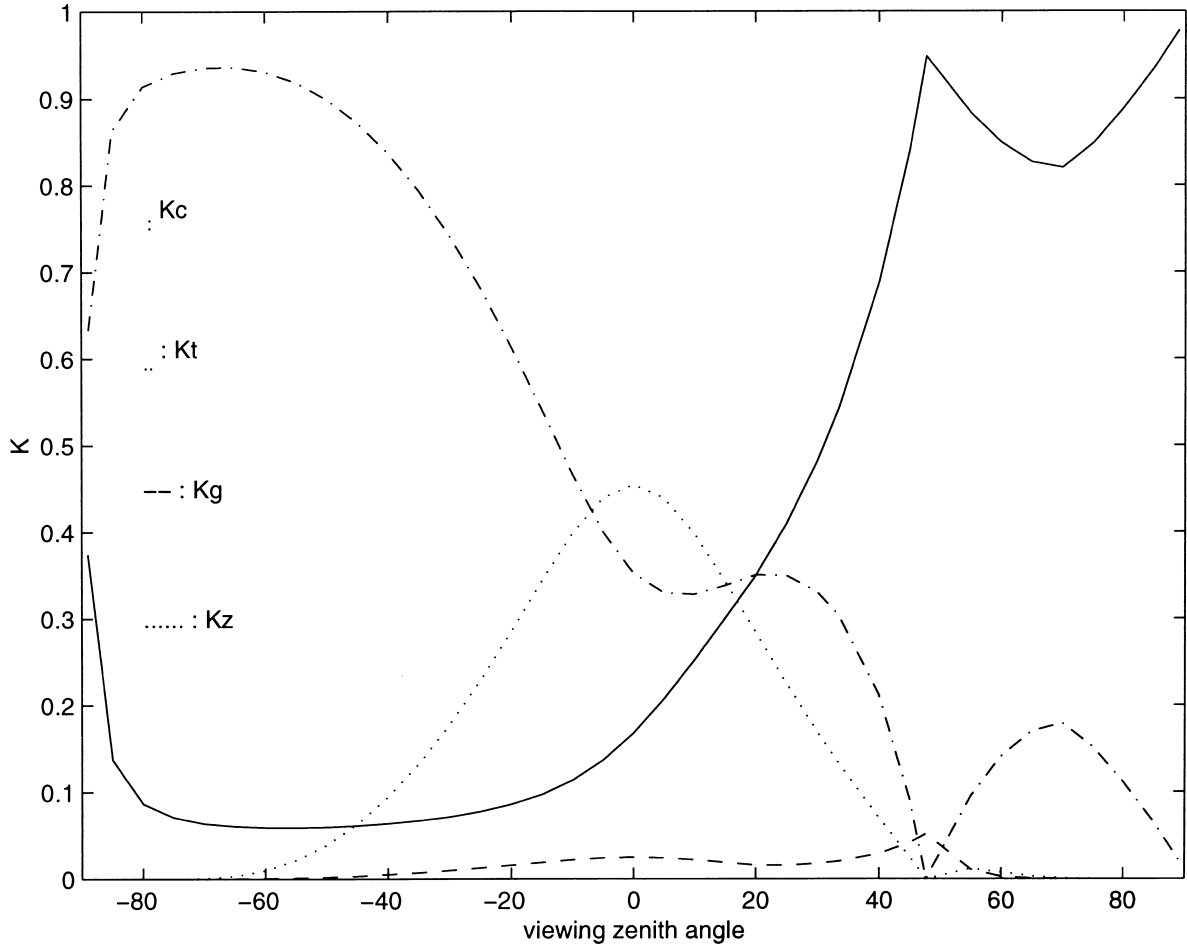


Figure 5. Areal proportions of the four scene components of the scene in the old black spruce (OBS) forest stand. The solar zenith angle is 47.7° .

In general, the expressions for $Var_s(r)$ are quite complex and must be computed numerically. Here for simplicity, we use the punctual variance $Var_s(k_g(i, v, \varphi)) = k_g(i, v, \varphi)(1 - k_g(i, v, \varphi))$ when the pixel size s is zero.

The two-component geometric optical (GO) BRVF model evolved from the full four-component pure GO model of Li and Strahler, so that the four spectral signatures of the four components in addition to the tree geometry parameters are the inputs of the model. In this study, the tree geometry parameters are listed in Table 2 from Ni et al., (1997) and Chen (1996); the spectral signature of sunlit background is from field measurements by Miller et al. (1997), and the spectral signatures of the other three components are chosen which best fit the BRDF values of the ASAS measurements. A use of these “best fit” values for the spectral signatures is less elegant than a modeling approach based on the tree geometry parameters and their spectral properties, such as was used in Ni et al. (1999), but was employed in an attempt to minimize the effect of errors in the estimates of component signatures on the predictions of BRVFs.

Figure 8 shows the comparison of the modeled

BRDF using the four component GO model and the modeled BRVF using the simple two-component GO model with the ASAS measurements. While the modeled results are far from a good fit, the model appears to capture the two primary features of the BRVFs: high values near nadir and the hotspot. The agreement is better in the red than the near-infrared spectral range, which is not surprising given the assumption that tree crowns are dark, like shadows, is more appropriate in the red. The most striking difference between the BRVF and the ASAS measurements is for the view angles between nadir and the hotspot. In fact, the modeled BRVF goes to zero, which is clearly not realistic. This situation can be explained by examining the behavior of the areal proportions and signatures of the two-components as a function of view angle.

Figure 9 shows the mean and variance of $k_g(i, v, \varphi)$ as a function of viewing zenith angles. Since $k_g(i, v, \varphi)$ is low (below 0.5) for all view angles, the variance of $k_g(i, v, \varphi)$ closely resembles the mean, as the variance is simply $k_g(i, v, \varphi)(1 - k_g(i, v, \varphi))$. The effect of this shape on the modeled BRVF (Fig. 8) is readily apparent.

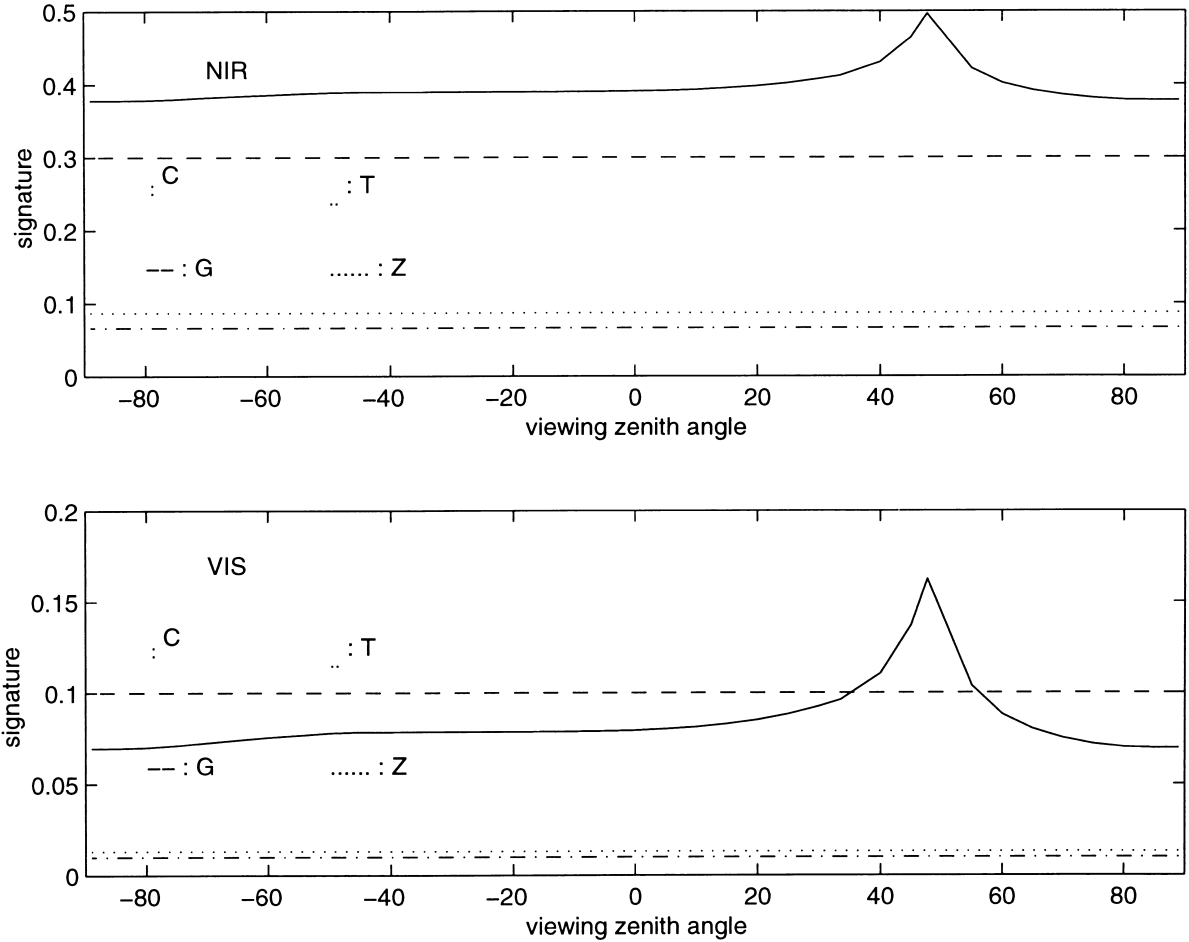


Figure 6. Spectral signatures of the four scene components of the scene in the old black spruce (OBS) forest stand. The solar zenith angle is 47.7° .

The second factor influencing the BRVF is the brightness difference between the two components, which is shown in Figure 10. Notice that the relative brightness of the two components changes greatly as a function of view angle, and between nadir and the hotspot they even cross. The point where they cross is where the BRVF goes to zero since the term $(G - X(i, v, \varphi))^2$ in Eq. (6) becomes zero. Note that this violates an original assumption of the model, which is that the background is bright and the tree/shadow composite component (X) is dark. The cross-over in component signatures is primarily the result of the background signature (G) being similar to the sunlit crown (C), which indicates there is an understory with significant amounts of green vegetation (Fig. 7).

Another interesting effect in the predicted BRVFs is that near nadir the highest values occur slightly toward the forward scattering direction (Fig. 8). This effect can also be understood from evaluation of the patterns of $k_g(i, v, \varphi)$ (Fig. 9) and the contrast in the brightness of G and $X(i, v, \varphi)$ (Fig. 10). While the variance of $k_g(i, v, \varphi)$ has a local peak at nadir, the contrast between G and $X(i, v, \varphi)$ continues to increase away from nadir in the

direction of forward scattering. The net result of these two effects is the highest variance in the angular region near nadir occurring slightly toward the forward scattering direction.

Figure 7. The four scene components used in the geometric optical mode: C is sunlit tree crown, T is shaded tree crown, G is sunlit background, and Z is shaded background.

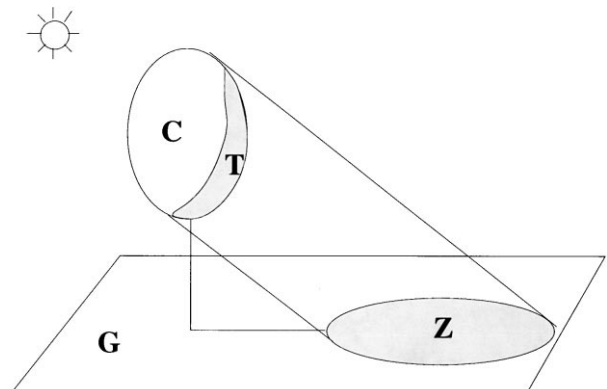


Table 2. Input Parameters for the Two-Component BRVF Model

Site	R (m)	b (m)	λ ($\frac{1}{m^2}$)	h	Δh (m)	C	G	T	Z
Red	0.76	2.7	0.41	5.75	5.5	0.12	0.1	0.01	0.01
NIR	0.76	2.7	0.41	5.75	5.5	0.42	0.3	0.08	0.09

R	Horizontal crown radius
b	Vertical crown radius
λ	Crown count density
h	Mean crown center height
Δh	Difference of upper and lower crown center height
C	Signature of sunlit crown
G	Signature of sunlit background
T	Signature of shaded crown
Z	Signature of shaded background

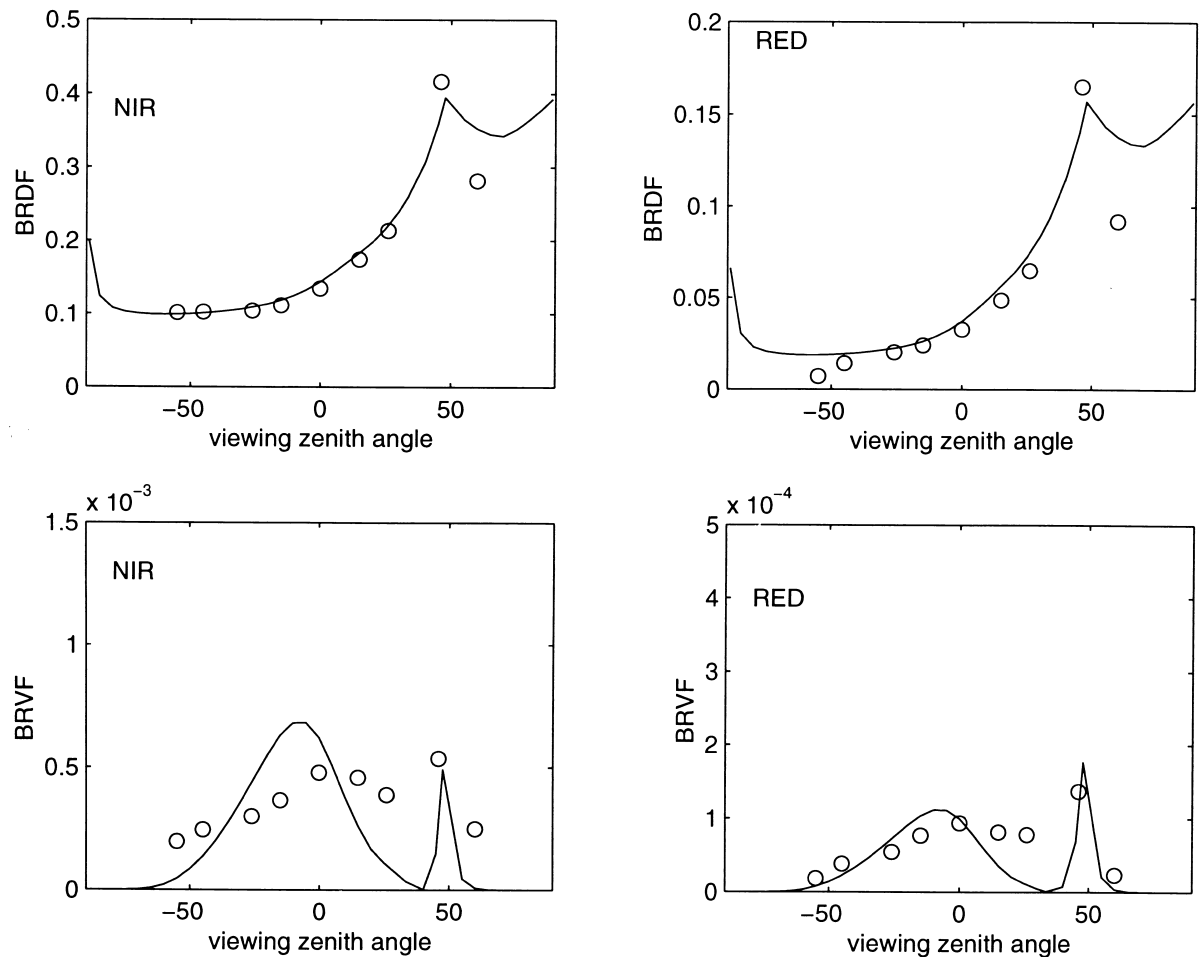
The Modified Two-Component Model

In an attempt to minimize the effects related to the crossover in component signatures described above, the two-component model was modified. The modification is based on the idea that the spectral signature of tree

crowns is more similar to the background than shadowed three crown or shaded background (Fig. 7).

The composite term, X is a mixture of sunlit crown C , shaded crown T , and shaded background Z . However, these three components are not of the same brightness,

Figure 8. Comparison of the modeled BRDF (solid line) using a GO model and field measurement (ASAS) (hollow) in the old black spruce forest stand in central Canada.



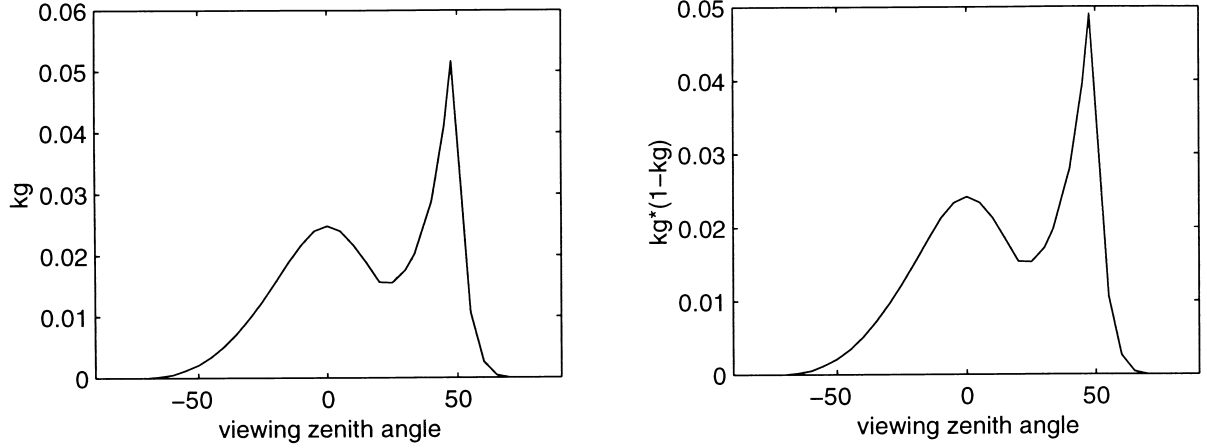


Figure 9. Modeled mean (left) and variance (right) of the areal proportion term, $k_g(i, v, \varphi)$.

and thus there will be a variance contribution from within the component X that is not included in the original two-component model. The idea of the modification is to add the effect of internal variance within X to the model. Here for simplicity, the shaded crown T and shaded background Z are taken as one component TZ and set as $TZ=(T+Z)/2$. Then the composite term x can be written as Eq. (7):

$$\begin{aligned} x(\theta_i, \theta_v, \varphi) &= \frac{k_c(i, v, \varphi)C + k_t(i, v, \varphi)T + k_z(i, v, \varphi)Z}{1 - k_g(i, v, \varphi)} \\ &= k'_c(i, v, \varphi)C + k'_{tz}(i, v, \varphi)TZ, \end{aligned} \quad (7)$$

where a lower case x indicates it is a variable rather than a constant, as X is in the two-component simple model. $k'_c(i, v, \varphi) = k_c(i, v, \varphi) / [1 - k_g(i, v, \varphi)]$, and $k'_{tz} = [k_t(i, v, \varphi) + k_z] / [1 - k_g(i, v, \varphi)] = 1 - k'_c(i, v, \varphi)$. The mean and variance of x can be written as Eqs. (8) and (9):

$$X(i, v, \varphi) = E(x(i, v, \varphi))$$

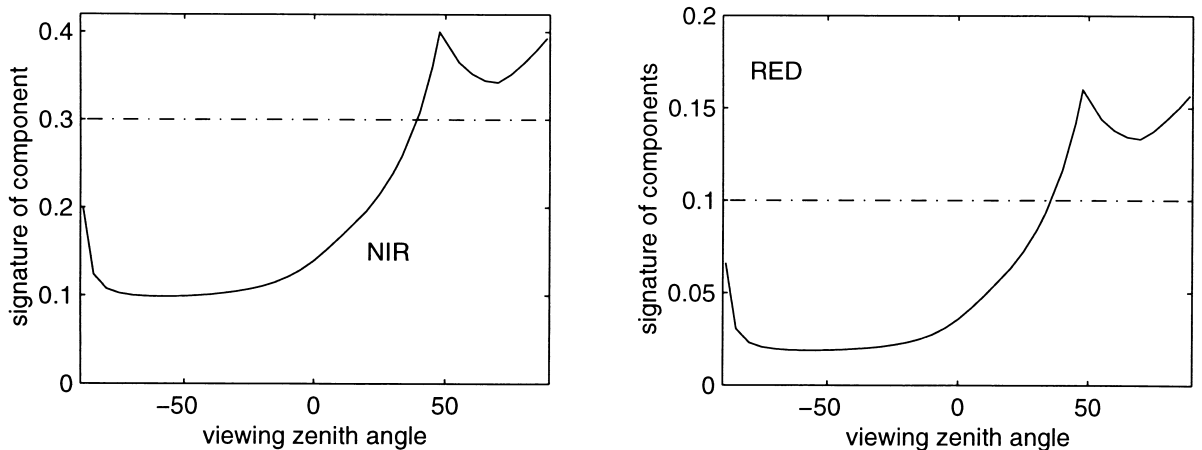
$$= K'_c(i, v, \varphi)C + K'_{tz}(i, v, \varphi)TZ, \quad (8)$$

$$\text{Var}(x(i, v, \varphi)) = (C - TZ)^2 \text{Var}(k'_c(i, v, \varphi)). \quad (9)$$

Figure 11 shows the mean, $K'_c(i, v, \varphi) \approx K_c(i, v, \varphi) / [1 - K_g(i, v, \varphi)]$, for the case of very small value of $k_g(i, v, \varphi)$, and $\text{Var}(k'_c) = K'_c(i, v, \varphi)(1 - K'_c(i, v, \varphi))$ with the change in view direction. The mean of k'_c again shows a bowl shape with the peak value at the hotspot. At the hotspot peak, K_{tz} goes to zero, as all shadows are hidden; with k'_c thus at 1, $\text{var}(k'_c)$ goes to zero. The peak between nadir and the hotspot in the forward scattering direction occurs as k'_c comes to equal K_{tz} and $\text{Var}(k'_c) = (0.5) * (0.5) = 0.25$. This peak corresponds to the region of obvious underestimation by the two-component model (Fig. 8).

Figure 12 shows the modeled mean and variance of the composite term x with the change of viewing zenith angle. The pattern of $\text{var}(x)$ is very similar to the patterns of $\text{var}(k'_c)$, with a peak value in the viewing direction when the two-component model predicts zero

Figure 10. The change of the spectral signatures of the two components (solid line for C and dash-dot line for G) with viewing zenith angle (left) and their differences (right).



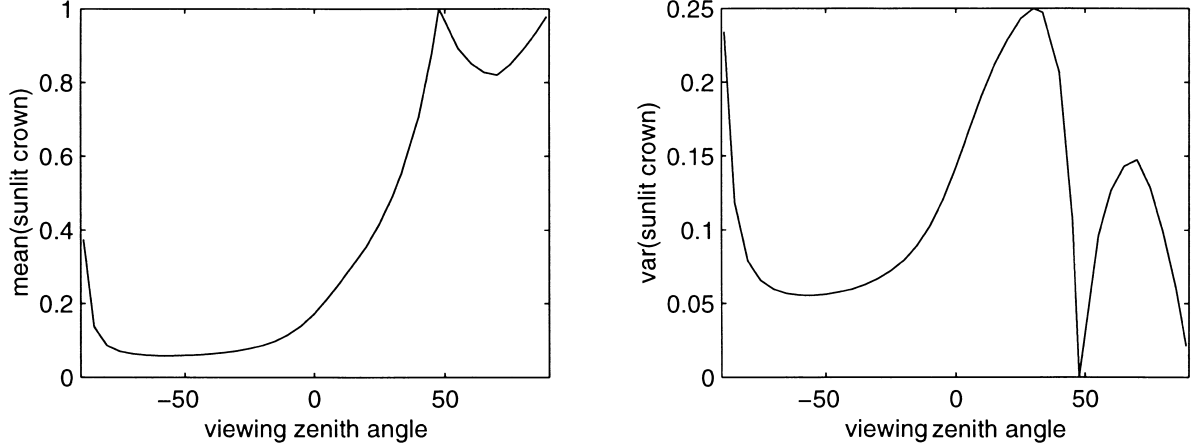


Figure 11. Mean (left) and variance (right) of the areal proportion term k'_c .

BRVF values due to constant values of C and TZ with the change of viewing zenith angle. The above shows that the two-component model can be improved by including the contribution of the contrast between the three components within the composite term in the two-component model.

In order to incorporate the variance of the composite term $x(i, v, \varphi)$ to the two-component model, the two-component model can be expressed as Eqs. (10) and (11):

$$r(i, v, \varphi) = k_g(i, v, \varphi)G + (1 - k_g(i, v, \varphi))x(i, v, \varphi) \\ = k_g(i, v, \varphi)G + x(i, v, \varphi) - k_g(i, v, \varphi)x(i, v, \varphi), \quad (10)$$

$$\text{Var}(r(i, v, \varphi)) = (G - X(i, v, \varphi))^2 \text{Var}(k_g(i, v, \varphi)) \\ + \text{Var}(k_g(i, v, \varphi)) \text{Var}(x(i, v, \varphi)) \\ + (1 - k_g(i, v, \varphi))^2 \text{Var}(x(i, v, \varphi)) \\ + (1 - k_g(i, v, \varphi))^2 \text{Cov}(k_g(i, v, \varphi), x(i, v, \varphi)). \quad (11)$$

To simplify this approximation, we note that usually $k_g(i, v, \varphi)$ and $x(i, v, \varphi)$ are negatively correlated, so that $\text{Cov}(k_g$

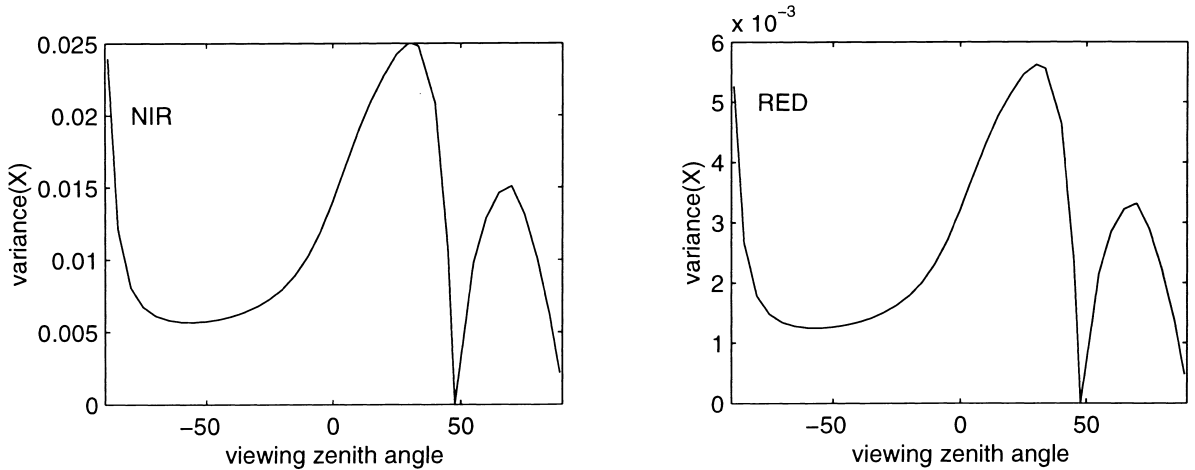
$(i, v, \varphi), x(i, v, \varphi)) \approx -\text{Var}(x(i, v, \varphi))$ and the last two terms in the above equation counterbalance each other. Thus $\text{Var}(r(i, v, \varphi))$ can be approximated as

$$\text{Var}(r(i, v, \varphi)) \approx (G - X(i, v, \varphi))^2 \text{Var}(k_g(i, v, \varphi)) \\ + \text{Var}(k_g(i, v, \varphi)) \text{Var}(x(i, v, \varphi)) \\ \approx (G - X(i, v, \varphi))^2 \text{Var}(k_g(i, v, \varphi)) \\ + (C - TZ)^2 \text{Var}(k_g(i, v, \varphi)) \text{Var}(k'_c(i, v, \varphi)) \quad (12)$$

Equation (12) shows the spatial variance of directional reflectance, $\text{Var}(r(i, v, \varphi))$, is a function of component signature differences $(G - X(i, v, \varphi))^2$ and $(C - TZ)^2$, variance of areal proportion terms, $\text{Var}(k_g(i, v, \varphi))$ and $\text{Var}(k'_c(i, v, \varphi))$. Ignoring the spatial resolution effect, $\text{Var}(k_g(i, v, \varphi)) = K_g(i, v, \varphi)(1 - K_g(i, v, \varphi))$, $\text{Var}(k'_c(i, v, \varphi)) = K'_c(i, v, \varphi)(1 - K'_c(i, v, \varphi))$.

Based on the geometric optics, the areal proportion terms change with solar and viewing geometry, as shown in Figure 5. Although the component signatures change with the solar zenith angles (Ni et al., 1998), the change

Figure 12. Variance of the composite term (X).



of areal proportion terms with the solar and viewing geometry is much larger than the change of component signatures. The pattern of the spatial variance of direction reflectance with the change of solar and viewing geometry is mainly controlled by the variance of areal proportion terms, $Var(k_g(i, v, \varphi))$, and $Var(k'_c(i, v, \varphi))$.

The changes of $Var(k_g(i, v, \varphi))$ and $Var(k'_c(i, v, \varphi))$ with the solar and viewing geometry depend on the values of $K_g(i, v, \varphi)$ and $K'_c(i, v, \varphi)$. The maximum value of $Var(k_g(i, v, \varphi))=0.25$ when $K_g(i, v, \varphi)=0.5$. When $K_g(i, v, \varphi)<0.5$, $Var(k_g(i, v, \varphi))$ increases with the increase of $K_g(i, v, \varphi)$; when $K_g(i, v, \varphi)>0.5$, $Var(k_g(i, v, \varphi))$ increases with the decrease of $K_g(i, v, \varphi)$. Similarly, the maximum value of $Var(k'_c(i, v, \varphi))=0.25$ when $K'_c(i, v, \varphi)=0.5$; when $K'_c(i, v, \varphi)<0.5$, $Var(k'_c(i, v, \varphi))$ increases with $K'_c(i, v, \varphi)$, and vice versa. For dense forest, such as the old black spruce forest in BOREAS are used in this study, $K_g(i, v, \varphi)<0.5$, $Var(k_g(i, v, \varphi))$ has the same pattern as $K_g(i, v, \varphi)$, with a maximum value at the hotspot and local maximum at nadir (Fig. 9), while $Var(k'_c(i, v, \varphi))$ has the maximum value at an angle between nadir and hotspot when $K'_c=0.5$ (Fig. 11).

Figure 13 shows the modeled mean and variance using the modified two-component model. It shows that the modified model does improve results, particularly at positive viewing zenith angles (or backward scattering), but is still too simple to match the data clearly.

For very dense forest, the pattern of BRVF with the change of solar and viewing geometry shows: 1) the peak value at hotspot and local peak value at nadir, due to the peak variance of $k_g(i, v, \varphi)$; 2) larger variance in backward scattering than forward scattering, due to the peak variance of $k_c(i, v, \varphi)/[1-k_g(i, v, \varphi)]$ in backward scattering. For very sparse forest, the pattern of BRVF with the change of solar and viewing geometry will differ from the case of dense canopy as we have shown in this study.

DISCUSSION

The first portion of this article shows four BRVFs for forest stands calculated from ASAS imagery. These BRVFs seem to indicate peak values at the hotspot and near nadir, but these findings are somewhat marginalized by poor sampling of the hotspot in some of the ASAS images. The value of these BRVFs derives primarily from their novelty, as to our knowledge only a single BRVF has been previously published. An improved understanding of BRVFs will require examination of many observed BRVFs, particularly those with measurements near the hotspot.

Spatial variation in images in a function of the spatial structure of the underlying scene. In open forests, shadowing effects of tree crowns as a function of the Sun and viewing directions create angular anisotropic variation in multiangular images. Meanwhile, spatial variation of multiangular images is also caused by variation of spectral

signatures of scene components and spatial variation of background and other scene components. In this study we ignore those variations since we believe those are much smaller than those between sunlit and shaded components.

The directional spatial variation of images can be explained in two ways. One is the BRVF, that is, the spatial variance of BRDF, as described in this study. The other is the directional effect on the height and the distance to the sill of the variogram as a function of the Sun and viewing directions at which the image is collected. Studies using variograms and local variance showed that the spatial variances of images are closely related to the size and density of scene objects. The tools developed in studies by Woodcock et al. (1988a,b) and Jupp et al. (1988; 1989) can be used and extended for multiangular images.

In the work presented here the punctual variance rather than a regularized variance is modeled. To study fully the relationship between BRVFs of ASAS images collected over discontinuous plant canopies and forest properties, accounting for the regularization effect is necessary. Two approaches can be used. One is to use the regularization tools developed by Jupp et al. (1988; 1989). Usually this is an exact approach, but it is complicated and numerical methods need to be applied. The other is using the deregularization tools developed by Collins (1998) to change the regularized variance to punctual variance. This is an empirical approach, but simple. Exploration of these approaches may benefit further work in applications of BRVF in multiangular imagery.

CONCLUSIONS

This study explores directional effects on the spatial variation of images over forests and how BRVF patterns are related to the properties of scene objects. This exploration was performed through analysis of multiangular images and modeling on an underlying scene model of discrete objects distributed on a contrasting background.

The BRVFs were calculated based on ASAS images collected at different boreal conifer stands. Overall the calculated BRVFs over different conifer stands show the following features: 1) the BRVF patterns with a function of viewing direction for different forest stands tend to have peak values around nadir and the hotspot. This feature is anticipated due to the effects of factors for discontinuous plant canopies—the geometric or shadowing effect and the regularization effect.

Jupp and Woodcock's simple two-component geometric optical (GO) mode for BRVF over discontinuous plant canopies was compared to ASAS images. This comparison shows that the simple model captures the basic features of maximum BRVF values around hotspot and nadir. Using the two-component model, the spatial variance of multiangular images is described by the variation

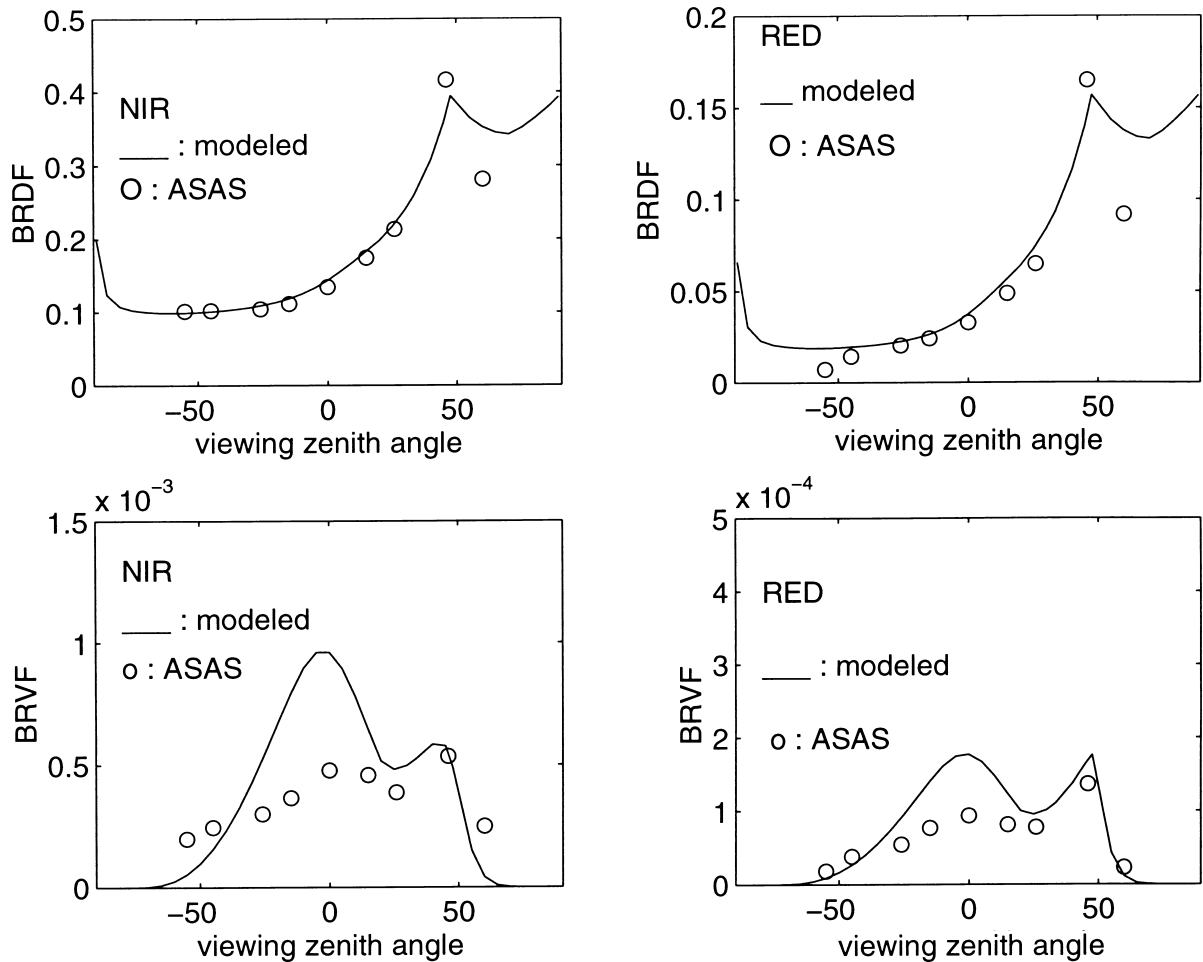


Figure 13. Comparison of the modeled BRDF using a GO model and BRVF using the modified two-component model with measurements (ASAS) from the old black spruce stand.

of sunlit background and the difference of the spectral signature of the sunlit background and the composite term.

This comparison also indicates some deviations of model prediction from the measurements. The cause of these deviation is contrast between more than two structure components contributes to the BRVFs. An improved version of this model was developed to account for the interaction of three scene components. The validation results show that the new model did improve the results, particularly for the viewing directions between nadir and the hotspot.

Using angular variations (the BRDF and BRVF) derived from multiangular remote sensing data offers the possibility of monitoring structural changes at a finer grain than image resolutions within broad mosaics of different covers. Also, the high spatial resolution data from airborne scanners and proposed civilian satellites will enhance the utility of image texture. One view of the BRVF uses the change in image texture as a function of illumination and viewing angles. At spatial resolutions where texture information is prominent, understanding

of the factors causing spatial variance in images will be critical.

This work is supported in part by U.S. Army Corps of Engineering under Contract DACA89-93-k-00012. The authors are in great debt to James R. Irons and his colleagues for collecting and providing ASAS data. We would like to thank three anonymous reviewers for their time and helpful comments which improved this manuscript.

REFERENCES

- Ardanuy, P. E., Han, D., and Salomonson, V. (1991), The Moderate Resolution Imaging Spectrometer (MODIS) science and data system requirements. *IEEE Trans. Geosci. Remote Sens.* 29:75–88.
- Bruniquel-Pinel, V., and Gastellu-Etchegorry, J. P. (1998), sensitivity of texture of high resolution images of forest to biophysical and acquisition parameters. *Remote Sens. Environ.* 65:61–85.
- Chen, J. M. (1996), Optically-based methods for measuring

- seasonal variation of leaf area index in boreal conifer stands. *Agric. For. Meteorol.* 80:135–163.
- Cohen, W. B., Spies, T. A., and Bradshaw, G. A. (1990), Semi-variograms of digital imagery for analysis of conifer canopy structure. *Remote Sens. Environ.* 34:167–178.
- Collins, J. (1998), Geostatistical methods for analysis of multiple scales of variation in spatial data. Ph.D. thesis, Department of Geography, Boston University.
- Dana, K. J., Ginneken, B., Nayar, S. K., and Koenderink, J. J. (1996), Reflectance and texture of real-world surfaces, Technical Report, Columbia University, New York (<http://www.cs.columbia.edu/CAVE/curet/index.html>).
- Deschamps, P. Y., Bréon, F. M., Leroy, M., et al. (1994), The POLDER mission: instrument characteristics and scientific objectives. *IEEE Trans. Geosci. Remote Sens.* 32:598–615.
- Diner, J. D., Bruegge, C. J., Martonchik, J. V., et al. (1989), MISR: Multiangle Imaging Spectroradiometer for geophysical and climatological research for EOS. *IEEE Trans. Geosci. Remote Sens.* 27:200–210.
- Gastellu-Etchegorry, J. P., Demarez, V., Pinel, V., and Zagolski, F. (1996), Modeling radiative transfer in heterogeneous 3-D vegetation canopies. *Remote Sens. Environ.* 58:131–156.
- Hardy, J. P., Davis, R. E., Jordan, R., Ni, W., and Woodcock, C. E. (1997), Snow ablation modeling in conifer and deciduous stands of the boreal forest. *Hydrol. Process.*, in press.
- Irons, J. R., Ranson, K. J., Irish, R. R., and Huegel, F. G. (1991), An off-nadir-pointing imaging Spectroradiometer for terrestrial ecosystem studies. *IEEE Trans. Geosci. Remote Sens.* 29:66–74.
- Jupp, D. L. B. (1997), Modeling directional variance and variograms using geo-optical models. *Remote Sens.* 1:101–107.
- Jupp, D. L. B., Strahler, A., and Woodcock, C. E. (1988), Autocorrelation and regularization in digital images: I. Basic theory. *IEEE Trans. Geosci. Remote Sens.* 26:463–473.
- Jupp, D. L. B., Strahler, A., and Woodcock, C. E. (1989), Autocorrelation and regularization in digital images: I. Simple image model. *IEEE Trans. Geosci. Remote Sens.* 27:247–258.
- Jupp, D. L. B., and Woodcock, C. E. (1992), Variance in directional radiance of open canopies. In *Proceedings of the IGARSS'92 Symposium: International Space Year: Space Remote Sensing*, pp 1490–1492.
- Li, X., and Strahler, A. H. (1985), Geometric-optical modeling of a conifer forest canopy. *IEEE Trans. Geosci. Remote Sens.* 23:705–721.
- Li, X., and Strahler, A. H. (1996), A knowledge-based inversion of physical BRDF models and three case studies. In *International Geoscience and Remote Sensing Symposium*, pp. 2173–2175.
- Miller, J. R., White, H. P., Chen, J. M., et al. (1997), Seasonal change in understory reflectance of boreal forests and influence on canopy vegetation indices. *J. Geophys. Res.* 102:29,475–29,482.
- Ni, W. (1997), Model development and application of the radiation regime within conifer forests, Ph.D. thesis, Department of Geography, Boston University.
- Ni, W., Li, X., Woodcock, C. E., Roujean, J. L., and Davis, R. (1997), Transmission of solar radiation in boreal conifer forests: measurements and models. *J. Geophys. Res.* 102(D24): 29,555–29,566.
- Ni, W., Li, X., Woodcock, C. E., Caetano, M. R., and Strahler, A. (1999), An analytical hybrid GORT bidirectional reflectance model and discontinuous plant canopies. *IEEE Trans. Geosci. Remote Sens.* 27:1–13.
- Schaaf, C., and Strahler, A. (1994), Validation of bidirectional and hemispherical reflectance from a geometric-optical model using ASAS imagery and pyranometer measurements of a spruce forest. *Remote Sens. Environ.* 49:138–144.
- Sellers P., Hall, F. M., Kelly, D. B., et al. (1995), The Boreal Ecosystem–Atmosphere Study (BOREAS): an overview and early results from the 1994 field year. *Bull. Am. Meteorol. Soc.* 76:1549–1577.
- Strahler, A. H. (1997), Vegetation canopy reflectance modeling—recent developments and remote sensing perspectives. *Remote Sens. Rev.* 15:179–194.
- Vermote, E. F., Tanré, D., Deuze, J. L., Herman, M., and Morcrette, J. J. (1997), Second simulation of the satellite signal in the solar spectrum: an overview. *IEEE Trans. Geosci. Remote Sens.* 35:675–686.
- Woodcock, C. E., Strahler, A., and Jupp, D. L. B. (1988a), The use of variograms in remote sensing: I. Scene models and simulated images. *Remote Sens. Environ.* 25:323–348.
- Woodcock, C. E., Strahler, A., and Jupp, D. L. B. (1988b), The use of variograms in remote sensing: I. Real digital images. *Remote Sens. Environ.* 25:349–379.
- Woodcock, C. E., Collins, J. B., Gopal, S., et al. (1994), Mapping forest vegetation using Landsat TM imagery and a canopy reflectance model. *Remote Sens. Environ.* 50:240–254.
- Woodcock, C. E., Collins J. B., Jakabhazy, V. D., Li, X., and Macomber, S. A. (1997), Inversion of the Li–Strahler model for mapping forest structure. *IEEE Trans. Geosci. Remote Sens.* 35(2):405–414.
- Wulder, M. A., LeDrew, E. F., Franklin, S. E., and Lavigne, M. B. (1998), Aerial image texture information in the estimation of northern deciduous and mixed wood forest leaf area index (LAI). *Remote Sens. Environ.* 64:64–76.